Research Article
Volume 11:06, 2022

Journal of Applied & Computational Mathematics

ISSN: 2167-0234 Open Access

Effect of Various Parameters on Velocity, Temperature and Concentration Distributions

Ayele Tulu[1*] and Wubshet Ibrahim[2]

[1]Department of Mathematics, Wollega University, Nekete, Ethiopia

[2]Department of Mathematics, Ambo University, Ambo, Ethiopia

Abstract

In this paper, the problem of unsteady two-dimensional mixed convection heat, mass transfer flow of nanofluid past a moving wedge embedded in porous media is considered. The effects of nanoparticle volume fraction, thermal radiation, viscous dissipation, chemical reaction, and convective boundary condition are studied. The physical problem is modeled using partial differential equations. The transformed dimensionless system of coupled nonlinear ordinary differential equations is then solved numerically using Spectral Quasi Linearization Method (SQLM). Effects of various parameters on velocity, temperature and concentration distributions as well as skin friction coefficient, local Nusselt number and local Sherwood number are shown using table and graphical representations. The results reveal that the nano fluid velocity and temperature profiles reduce with increasing the values of nanoparticle volume fraction. Greater values of temperature and concentration distributions are observed in the steady flow than unsteady flow. The skin friction coefficient and local Sherwood number are increasing functions while the local Nusselt number is a decreasing function of nanoparticle volume fraction, permeability parameter, Eckert number, Dufour number, and Soret number. The obtained solutions are checked against the previously published results and a very good agreement have been obtained.

Keywords: Unsteady • Mixed convection • Wedge flow • Nanofluid • Porous media

Introduction

In the past few years, researchers have continuously worked on developing innovative heat transfer fluids that have significantly greater thermal conductivities than usually used fluids. In 1995, Choi was the first scholar who developed a newly pioneering type of heat transfer fluids and for such form of fluids he gave the term “nanofluids”. He prepared these fluids on sagging nanoscale particles of metallic basis with particle size less than 100 nm in a common heat transfer fluids [1]. Nanofluids have been getting high attention in recent years not only due to higher in thermal conductivity but also potentially worthwhile in many modern-day applications. These include microelectronics, fuel cells, food processing, biomedicine, power generation, ventilation, engine vehicle management, domestic refrigerator, and heat exchanger. Some of the studies on boundary layer flow of nano fluid past a wedge. Their study revealed that heat and mass transfer rates are reduced with increasing the value of pressure gradient parameter. The flow of Cu-Water and Ag-Water nano fluids past a porous wedge with the influences of MHD was considered. They showed that dual solutions happen for the negative pressure gradient.

The flow of fluid through porous media is essential due to its application in material sciences and engineering such as Petroleum industries, seepage of water in riverbeds, filtration and purification of chemical processes and many others. The analysis of boundary layer flow past a wedge in porous media has been a subject of several research papers [2]. MHD boundary layer flow past a fixed wedge within porous media was considered. Unsteady MHD boundary layer flow of nanofluid and heat transfer past a moving wedge in a porous medium. They concluded that presence of porous parameter is helpful to generate heat in the system. Mixed convection flow is vital when the buoyancy force is created due to temperature variation between the solid surface and free stream grows, and which in turn considerably affect the flow and the thermal fields. This flow arises in different transport processes such as heat exchangers, solar collectors, nuclear reactors, ground water pollution, and electronic equipment. Mixed convection boundary layer flow in a porous medium was investigated [3].

Viscous dissipation is the heat energy that is created as a result of friction between fluid layers. It alters the temperature flow distribution by acting like an energy source which indicts to affect the amount of heat transfer. MHD heat and mass transfer flow of nano fluids with the effects of viscous dissipation. The effects of viscous dissipation on MHD flow of nano fluid past a fixed wedge embedded in porous media. They noticed that an increment in Eckert number leads to enhance the temperature distributions [4]. It is remarkable that radiation heat transfer can occur between two bodies separated by a medium colder than both bodies. For example, solar radiation reaches the surface of the earth after passing through cold air layers at high altitudes. At high temperatures, radiation significantly affects temperature distribution and heat transfer. The effect of thermal radiation on mixed convection flow of Nano fluid flow over a stretching sheet was examined and analyzed the effect of solar radiation on Ag-water nano fluid flow over an inclined porous plate embedded in a porous medium. They revealed that heat transfer coefficient increases with increasing radiation parameter. Chemical reactions are happened in numerous mass transfer problems, and it results in the generation of a species. The flow of fluid is also affected by chemical reactions that take place in it. The effect of chemical reaction on MHD flow

***Address for Correspondence:** Ayele Tulu, Department of Mathematics, Wollega University, Nekete, Ethiopia; Tel: 251 0911776212; E-mail: ayeletulu@gmail.com*

Received: 09 Sep, 2019, Manuscript No. JACM-19-2313; **Editor assigned:** 13-Sep, 2019, PreQC No. P- JACM-19-2313; **Reviewed:** 27 Sep, 2019, QC No. Q-JACM-19-2313 **Revised:** 02 Sep, 2022, QI No. Q- Sep-19-2313; Manuscript No. R-JAMC-19-19-2313; **Published:** 13 Oct, 2022, DOI: 10.37421/ 2168-9679.2022.11.480

of nano fluids past a wedge through porous medium was analyzed. Their result revealed that mass transfer rate at the boundary surface increases with increasing chemical reaction parameter [5].

The study of unsteady mixed convection heat and mass transfer flow of nano fluid past moving wedge embedded in a porous medium has not been given much consideration so far. Analyzing the effects of unsteady parameter, moving wedge parameter, and convective boundary condition of mixed convection heat and mass transfer flow using Spectral Quasi Linearization Method (SQLM) makes this study novel [6]. Further, we considered nono fluids of Cu, Ag and Al_2O_3 nanoparticles with H_2O as a base fluid. Employing SQLM are advantageous due to its fast convergence, easy to implement, adaptable to various problems, provide more accurate approximations with a relatively small number of unknowns, and require less grid points to achieve accurate results. The effects of different parameters on velocity, temperature, and concentration fields as well as the skin friction coefficient, the local Nusselt number, and the local Sherwood number are analyzed with the help of table and graphical representations [7,8].

Methodology

Mathematical formulation

We considered unsteady two-dimensional laminal mixed convection heat and mass transfer boundary layer flow of nano fluid past a moving wedge embedded in a porous medium [8,9]. It is assumed that the coordinate system is chosen with x corresponding to the plane in the course of the flow and y indicating towards the free stream as shown in Figure 1 below.

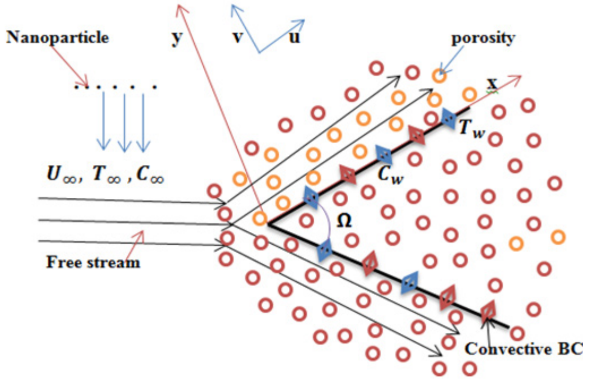

Figure 1. Physical model and coordinate system.

It is also presumed that wedge is moving with velocity $u_w(x,t)=\frac{U_w}{1-\gamma t}x^m$ and the velocity of the potential flow is $u(x,t)=\frac{U_w}{1-\gamma t}x^m$. The wall of the wedge is kept with variable temperature $T_w(x,t)=T_\infty+T_0(\frac{x}{1-\gamma t})^{2m}$ and variable nanoparticle concentration $C_w(x,t)=C_\infty+C_0(\frac{x}{1-\gamma t})^{2m}$, where T_0, C_0, $T\infty$, and $C\infty$ are reference temperature, reference concentration, ambient temperature, and ambient nanoparticle concentration respectively. $\gamma \geq 0$ are constants, t is time and $\gamma t<1$, x is measured from the tip of the wedge, m is the Falkner-Skan power-law parameter. Further, the buoyancy force caused by temperature and concentration variation inside moving fluid is considered, and are taken in momentum equation [9-11]. The effects of thermal radiation, viscous dissipation, chemical reaction, and convective boundary condition are also encompassed in present study.

Using the above assumptions and the boundary layer approximation the continuity, momentum, energy, and nanoparticle concentration equations governing the considered problem are given as

$$\frac{\partial u}{\partial x}+\frac{\partial v}{\partial y}=0 \tag{1}$$

$$\frac{\partial u}{\partial t}+u\frac{\partial u}{\partial x}+v\frac{\partial u}{\partial y}=-\frac{1}{\rho_{nf}}\frac{\partial p}{\partial x}+v_{nf}\frac{\partial^2 u}{\partial y^2}-\frac{V_{nf}}{K}u+g\beta_T(T-T_\infty)+g\beta_c(C-C_\infty) \tag{2}$$

$$\frac{\partial T}{\partial t}+u\frac{\partial T}{\partial x}+v\frac{\partial T}{\partial y}=\alpha_{nf}\frac{\partial^2 T}{\partial y^2}+\frac{v_{nf}}{C_{pnf}}(\frac{\partial u}{\partial y})^2-\frac{1}{(\rho C_p)}\frac{\partial q_r}{\partial y}+\frac{\rho_f D_m K_T}{C_s(\rho C_p)_{nf}}\frac{\partial^2 C}{\partial y^2} \tag{3}$$

$$\frac{\partial C}{\partial t}+u\frac{\partial C}{\partial x}+v\frac{\partial C}{\partial y}=D_B\frac{\partial^2 C}{\partial y^2}+\frac{D_m K_T}{T_m}\frac{\partial^2 T}{\partial y^2}-k_r(C-C_\infty) \tag{4}$$

The suitable boundary conditions are given as:

$$\begin{aligned}
&t<0;\ u=0;\ v=0;\ T=T_\infty;\ C=C_\infty\ \forall_{x,y}\\
&T \geq 0:\ u=u_w(x,t)=\frac{U_w}{1-\gamma t}x^m\\
&v=0;\ k_f\frac{\delta T}{\delta y}=-h_f(T_w-T)\\
&D_m\frac{\partial C}{\partial y}=-h_s(C_w-C)\\
&u\to U(x,t)=\frac{U_\infty}{1-\gamma t}x^m\\
&T\to T\infty;\ C\to C\infty \text{ as } y\to\infty
\end{aligned} \tag{5}$$

Where u and v denote the x and y velocity components respectively. ρ_f, ρ_{nf} , ν_{nf} , α_{nf} , and $(C_p)_{nf}$ are density of base fluid, effective density, effective kinematic viscosity, effective thermal diffusivity, and effective specific heat capacity of the nano fluid respectively [12,13]. Likewise, g, β_T, β_C, K, q_r, D_m, K_T, C_s, T_m, D_B and k_r are respectively acceleration due to gravity, volumetric coefficient of thermal expansion, volumetric coefficient of concentration expansion, permeability of porous medium, radiation heat flux, mass diffusivity, thermal diffusion ratio, concentration susceptibility, mean fluid temperature, Brownian diffusion coefficient, and rate of chemical reaction. Moreover, $h_f(x,t)=h_0x^{\frac{m-1}{2}}(1-\gamma t)^{-\frac{1}{2}}$ and $h_s(x,t)=h_1x^{\frac{m-1}{2}}(1-\gamma t)^{-\frac{1}{2}}$ are convective heat and mass transfer coefficients respectively where h0 and h1 being constants. The expression U, u_w, T_w, C_w, h_f, and h_s are usable for $t>\gamma^{-1}$.

For a uniform stream, the pressure term in the momentum equation (2) defined as:

$$-\frac{1}{\rho_{nf}}\frac{\partial p}{\partial x}=\frac{dU}{dt}+U(\frac{dU}{dx}+\frac{v_{nf}}{K}) \tag{6}$$

Employing the Rosseland approximation, the radiative heatflux qr term in the energy equations is given by:

$$q_r=-\frac{16T_\infty^3\sigma^*}{3k^*}\frac{\partial T}{\partial y} \tag{7}$$

where σ^* is the Stefan-Boltzmann constant and k^* is the mean absorption coefficient. The nanofluid effective thermo physical properties are given as:

$$\rho_{nf}=\phi_v\rho_s+(1-\phi_v)\rho_f\ ;\ (C_p)_{nf}=\phi_v(\rho C_p)_s+(1-\phi_v)(\rho C_p)_f \tag{8}$$

$$\mu_{nf}=\frac{\mu_f}{(1-\phi_v)^{2.5}};\ v_{nf}=\frac{\mu_{nf}}{\rho_{nf}}=\frac{v_f}{\phi_1}\quad \alpha_{nf}=\frac{k_{nf}}{(\rho Cp)_{nf}}=\frac{k_{nf}}{\phi_2(\rho Cp)_f} \tag{9}$$

where ν, ρ_s, ρ_f, $(C_p)_s$, $(C_p)_f$, μ_f , and ν_f are respectively the nanoparticle volume fraction, density of nanoparticle, density of base fluid, specific heat capacity of nanoparticle, specific heat capacity of base fluid, dynamic viscosity, and kinematic viscosity of the base fluid, where the nanoparticle volume fraction $\varphi 1$ and $\varphi 2$ are defined as

$$\phi_1=(1-\phi_v)^{2.5}[1-\phi_v+\phi_v\frac{\rho_s}{\rho_f}];\quad \phi_2=1-\phi_v+\phi_v\frac{(\rho Cp)_s}{(\rho Cp)_f} \tag{10}$$

The effective thermal conductivity k_{nf} of nanofluids when the added particles are of spherical shape, low volume percent, and the suspension is at ambient conditions is defined using the thermal conductivities of both nanoparticles k_s and basefluid k_f as

$$k_{nf}=k_f\frac{(k_s+2k_f)-2\phi_v(k_f-k_s)}{(k_s+2k_f)+\phi_v(k_f-k_s)} \tag{11}$$

It is also recognized that the base fluid and the nanoparticles are in thermal equilibrium and no slip take place between them. The thermophysical properties of the nanofluid for Cu, Ag, and Al_2O_3 nanoparticles and H_2O as base fluid are given in Table 1.

Table 1. Thermo-physical properties of base fluid and nanoparticles.

Physical properties	H_2O	Ag	Cu	Al_2O_3
Cp (J/kgK)	4179	235	385	765
ρ(kg/m3)	997.1	10500	8933	3970
k(W/mK)	0.613	429	401	40
α × 107 (m2/s)	1.47	1738.6	1163.1	-
β × 105 (K−1)	21	1.89	1.67	0.85

We introduce the stream function ψ which is defined as $u=\frac{\partial\psi}{\partial y}$ and $v=-\frac{\partial\psi}{\partial x}$ and the dimensionless similarity variables.

$$\eta = y\sqrt{\frac{1+m}{2}\frac{U_\infty}{v_f(1-\gamma t)}}x^{\frac{m-1}{2}};\ \psi(\eta) = \sqrt{\frac{2}{1+m}\frac{v_f U_\infty}{1-\gamma t}}x^{\frac{m+1}{2}}f(\eta)$$

$$\theta(\eta) = \frac{T-T_\infty}{T_w-T_\infty};\ \theta(\eta) = \frac{C-C_\infty}{C_w-C_\infty} \tag{12}$$

Thus, the continuity equation (1) is identically fulfilled, and upon substituting similarity variables into equations (2)-(5), we obtain the following system of coupled nonlinear ODEs:

$$f''' + \phi_1[ff'' + \beta(1-(f')^2) + \frac{A}{m+1}(2-\eta f'' - 2f') + \frac{2}{1+m}(Gr_t\theta + Gr_c\phi)] + \frac{1}{m+1}\kappa(1-f') = 0 \tag{13}$$

$$(\frac{1}{\Pr}\frac{k_{nf}}{k_f} + Nr)\theta'' + \phi_2[f\theta' - 2\beta f'\theta - A(\frac{\eta}{1+m}\theta' + 2\beta\theta)] + D_f\phi'' + \frac{E_c}{(1-\phi_v)^{2.5}}(f'')^2 = 0 \tag{14}$$

$$\frac{1}{Sc}\phi'' + f\phi' - 2\beta f'\phi - A(\frac{\eta}{1+m}\phi' + 2\beta\phi) + Sr\theta'' - \frac{2}{1+m}r_c\phi = 0 \tag{15}$$

The transformed boundary conditions are given as:

f(0)=0; f'(0)=λ; θ'(0) = -Bi1 (1-θ(0)); φ'(0) = -Bi2 (1-φ(0)) f'(∞) $\longrightarrow$ 1; $\theta(\infty)$ $\longrightarrow$ 0; $\varphi(\infty)$ $\longrightarrow$ 0 (16)

$$\beta = \frac{2m}{1+m};\ A = \frac{\gamma}{U_\infty}x^{1-m}$$

$$\kappa = \frac{2v_f}{KU}x;$$

$$Gr_t = \frac{g\beta_T(T_w-T_\infty)}{U^2}x;$$

$$Gr_c = \frac{g\beta_C(C_w-C_\infty)}{U^2}x;$$

$$\Pr = \frac{v_f}{\alpha_f};$$

$$Sc = \frac{v_f}{D_B};$$

$$Ec = \frac{U^2}{(C_p)_f(T_w-T_\infty)};$$

$$Nr = \frac{16\sigma^* T_\infty^{\ 3}}{3k^* v_f(\rho C_p)_{nf}};$$

$$S_r = \frac{D_m K_T}{v_f T_m}\frac{T_w-T_\infty}{C_w-C_\infty};$$

$$D_f = \frac{\rho_f D_m K_T}{v_f C_s(\rho C_p)nf}\frac{C_w-C_\infty}{T_w-T_\infty};$$

$$r_c = \frac{k_r}{U}x^{-1};$$

$$\lambda = \frac{U_w}{U_\infty};$$

$$Bi_1 = \frac{h_0}{k_f}(\frac{2v_f}{(1+m)U_\infty})^{1/2};$$

$$Bi_2 = \frac{h_1}{D_B}(\frac{2v_f}{(1+m)U_\infty})^{1/2}$$

Here, β, λ, A, κ, Grt, Grc, Pr, Ec, Sc, Df, Nr, Sr, rc, Bi1 and Bi2 are respectively the Hartree pressure gradient parameter, moving wedge parameter, unsteady parameter, permeability parameter, local temperature Grashof number, local concentration Grashof number. Prandtl number, Eckert number, Schmidt number, Dufour number, thermal radiation parameter, Soret number, scaled chemical reaction parameter, and Biot numbers and prime [14-19].

The skin friction coefficient Cf, local Nusselt number Nux, and local Sherwood number Shx are the three important physical quantities in engineering and it is defined as:

$$C_f = \frac{2\tau_w}{\rho_f U^2(x,t)};\ \mathrm{Nu}_x = \frac{xq_w}{k_f(T_w-T_\infty)}\quad Sh_x = \frac{xM_w}{D_B(C_w-C_\infty)} \tag{17}$$

Where $\tau_w = -\mu_{nf}(\frac{\partial u}{\partial y})_{y=0}$ the surface is shear stress, $q_w = -k_{nf}(\frac{\partial T}{\partial y})_{y=0}$ is the surface heat flux and $M_w = -D_B(\frac{\partial C}{\partial y})_{y=0}$ is surface mass flux. Hence, the non-dimensional skin friction coefficient, local Nusselt number, and local Sherwood number are respectively given as:

$$\frac{1}{2}(1-\phi_v)^{2.5}\sqrt{\frac{2}{1+m}}C_f\sqrt{\mathrm{Re}_x} = -f''(0) \tag{18}$$

$$\frac{k_f}{k_{nf}}\sqrt{\frac{2}{1+m}}\frac{Nu_x}{\sqrt{\mathrm{Re}_x}} = -\theta'(0);\ \sqrt{\frac{2}{1+m}}\frac{Sh_x}{\sqrt{\mathrm{Re}_x}} = -\phi'(0) \tag{19}$$

where Rex is local Reynolds number defined by $\mathrm{Re}_x = \frac{U_x}{v_f}$

Numerical method

In this section, the system of non-linear ODE (13)-(15) subject to the boundary conditions (16) are solved numerically using SQLM [20,21]. The central point behind this method is identifying nonlinear component of a differential equation, linearizing the terms using the multivariate Taylor series expansion and applying Chebychev pseudo-spectral collocation method [22].

Employing SQRM on equations (13)-(15), the following iterative scheme of linear differential equations is found.

$$f_{r+1}''' + \phi_1(f_r - \frac{A}{1+m}\eta)f_{r+1}'' - (2\phi_1(\beta f_r' + \frac{A}{1+m}) + \frac{k}{1+m})f_{r+1}' + \phi_1 f_r'' f_{r+1} + \frac{2}{1+m}$$

$$\phi_1 Gr_t\theta_{r+1} + \frac{2}{1+m}\phi_1 Gr_c\phi_{r+1} = \phi_1(f_r f_r'' - \beta(1+(f_r')^2)) - \frac{1}{1+m}(2A\phi_1 + k) \tag{20}$$

$$(\frac{1}{\Pr}\frac{k_{nf}}{k_f} + Nr)\theta_{r+1}'' + \phi_2(f_r - \frac{A}{1+m}\eta)\theta_{r+1}' - 2\beta\phi_2(f_2' + A)\theta_{r+1} + \phi_2\theta_r' f_{r+1} -$$

$$2\beta\phi_2\theta_r f_{r+1}^1 + \frac{2Ec}{(1-\phi_v)^{2.5}}f_r'' f_{r+1}'' + D_f\phi_{r+1}'' = \phi_2(f_r\theta_r' - 2\beta f_r'\theta_r) + \frac{E_c}{(1-\phi_v)^{2.5}}(f_r'')^2 \tag{21}$$

$$\frac{1}{Sc}\phi_{r+1}'' + (f_r - \frac{A}{1+m}\eta)\phi_{r+1}' - 2(\beta(f_r' + A) + \frac{1}{1+m})$$

$$\phi_{r+1} + \phi_r' f_{r+1} - 2\beta\phi_r f_{r+1}' + Sr\theta_{r+1}'' = f_r\phi_r' - 2\beta f_r'\phi_r \tag{22}$$

With transformed corresponding boundary conditions

fr+1(0)=0; f'r+1(0)=λ ; θ'r+1(0) = -Bi1(1-θ (0)); ϕ'r+1(0) = –Bi2(1-ϕ (0))

f'r+1(∞) $\longrightarrow$ 1; θr+1(∞) $\longrightarrow$ 0; ϕr+1(∞) $\longrightarrow$ 0 (23)

where the terms r+1 and rare at the current and previous iteration levels respectively.

Equations (20)-(22) are then solved using the Chebyshev pseudo-spectral method. The unknown functions are given by Chebyshev interpolating polynomials with Gauss Lobatto points that are defined by CSP method.

ξj = cos(π j/N), j = 0, 1, 2, ..., N; $-1 \le \xi \le 1$ (24)

where N is the number of collocation points used. Using the linear transformation $\xi = \frac{2\eta}{L_\infty} - 1$ the interval (0, L∞) is transformed into the interval (-1, 1) where L∞ is large but finite number chosen to represent the behavior of the flow properties of the boundary condition value at infinity. Discretizing the system of equations (20)-(22) using spectral collocation method [23,24]. The differentiation matrix $D = \frac{2D}{L_\infty}$ is used to approximate derivatives of unknown variables where D is (N+1) × (N+1) Chebyshev differentiation matrix. The system of equations (20)-(22) are then solved as a coupled matrix:

$$\begin{pmatrix}\Lambda_{11} & \Lambda_{12} & \Lambda_{13}\\ \Lambda_{21} & \Lambda_{22} & \Lambda_{23}\\ \Lambda_{31} & \Lambda_{32} & \Lambda_{33}\end{pmatrix}\begin{bmatrix}F_{r+1}\\ \Theta_{r+1}\\ \Phi_{r+1}\end{bmatrix} = \begin{bmatrix}B_1\\ B_2\\ B_3\end{bmatrix}$$

With transformed boundary condition

$$F_{r+1}(\xi_N) = 0, F_{r+1}(\xi_{N-1}) = \lambda, F_{r+1}(\xi_0) = 1, \Theta_{r+1}(\xi_N) = -Bi_1(1-\theta(0)), \Theta_{r+1}(\xi)_0 = 0, \Theta_{r+1}(\xi_N) = -Bi_2(1-\phi(0)), \Theta_{r+1}(\xi_0) = 0$$

where $\Lambda_{11} = D^3 + \phi_1 diag[f_r - \frac{A}{1+m}\eta]D^2 - 2\beta\phi diag[\mathrm{f}_r^1]D - \frac{1}{1+m}(2\phi A + k)D + \phi_1 diag[f_r'']$ (26)

$$\Lambda_{12} = \frac{2}{1+m}\phi_1 Gr_t I;\qquad \Lambda_{13} = \frac{2}{1+m}\phi_1 Gr_c I$$

$$\Lambda_{21} = \frac{2E_c}{(1-\phi_v)^{2.5}}diag[f_r'']D^2 - 2\beta\phi_2 diag[\theta_r]D + \phi_2 diag[\theta_r']$$

$$\Lambda_{22} = (\frac{R}{\Pr} + Nr)D^2 + \phi_2 diag[f_r - \frac{A}{1+m}\eta]D - 2\beta\phi_2 diag[f_r' + A];\ \Lambda_{23} = D_f D^2$$

$$\Lambda_{31} = -2\beta diag[\phi_r]D + diag[\phi_r'];\ \Lambda_{32} = S_r D^2$$

$$\Lambda_{33} = \frac{1}{Sc}D^2 + diag[f_r - \frac{A}{1+m}\eta]D - 2\beta diag[f_r' + A] - \frac{2}{1+m}Y_c I$$

$$B_1 = \phi[f_r'' f_r - \beta(1+(f_r')^2)] - \frac{1}{1+m}(2A\phi_1 + k)$$

$$B_2 = \phi_2(f_r\theta_r' - 2\beta f_r'\theta_r) + \frac{Ec}{(1-\phi_v)^{2.5}}(f_r'')^2;\qquad B_3 = fr\phi_r' - 2\beta f_r'\phi_r$$

$F_{r+1} = [f_{r+1,0}, F_{r+1,1}, --- _{r+1,N},]^T$ Are vectors of sizes (N+1) × 1, diag (...) represents a diagonal matrix of vectors, and I is an identity matrix of size (N+1) × (N+1). When SQLM is used the choice of an initial guess is very essential. The success of the scheme depends prominently on how good this guess is to give the most accurate solution [25]. The suitable initial guesses that satisfy the governing boundary conditions (13)-(16) are:

$$f_0(\eta) = \eta - 1 + e^{-(1-\lambda)\eta};\quad \theta_0(\eta) = \frac{Bi_1}{1+Bi_1}e^{-\eta};\quad \phi_0(\eta) = \frac{Bi_2}{1+Bi_2}e^{-\eta}; \tag{27}$$

Results and Discussion

The results of this study are obtained using the SQRM with the number of collocation points N=50 in the space ξ and the scaled parameter η=6 in all cases. Unless it is specified the parameters value used to produce the results are β=0.5, δ=0.10, κ=0.5, Pr=6.2, Sc=1, A=0.8, Ec=0.2, Df=0.2, Sr=0.3, Grt=Grc=0.01, λ=0, c=0.3, Bi1=Bi2=0.5 [26]. The values of these parameters are taken based on the average values of base fluid at ambient condition. The results are obtained for the velocity, temperature, and concentration profiles as well as the skin friction coefficient, local Nusselt number, and local Sherwood number using various parameters. Tables 2 and 3 respectively show the skin friction coefficient -f”(0) for various values of m, and the local Nusselt number -θ’(0) for numerous values of Pr which are respectively compared with previously published results of and [26]. Keeping the rest parameters value remain constant. Here, a very good agreement is realized which in turn confirm the accuracy of the present solutions (Tables 2 and 3).

Table 4 shows the skin friction coefficient, local Nusselt number, and local Sherwood number for Cu, Ag and Al_2O_3 water based nanofluids with various values of unsteadiness parameter A and nanoparticle volume fraction ν when the other parameters value remain the same (Table 4).

Here, it is shown that the skin friction coefficient, local Nusselt number, and local Sherwood number are increasing functions of A. For Cu and Ag water based nanofluids, as ν increases, the skin friction coefficient and local Sherwood number increase while the local Nusselt number reduces [27,28].

Moreover, for Al_2O_3 water based nanofluids, the skin friction coefficient, local Nusselt number, and local Sherwood number are decreasing functions of ν. Table 5 shows the calculated values of the skin friction coefficient, the local Nusselt number and local Sherwood number for both Ag and Al_2O_3 water based nanofluids when ν=0.1, Pr=6.2, Sc=1, A=0.8, λ=0.1, Grt=Grc=0.01, Bi1=Bi2=0.5 for some values of β, κ, Nr, Ec, Yc, Df and Sr (Table 5).

Table 2. Comparison of the SQLM results of skin friction coefficient -f “(0) for normal fluid (φ_v=0) for various values of m when Pr=0.73, Sc=1, λ=Sr=Df=Grt=Grc=Ec=Yc=Nr=κ=A=0.

			− f “(0)		
m	**Ashwini et al.**	**Watanaba**	**Ullah et al.**	**Ganapathirao et al.**	**Present**
0	0.4696	0.4696	0.4696	0.46972	0.4696
0.0141	0.5046	0.50461	0.5046	0.50481	0.50461
0.0435	0.569	0.56898	0.569	0.5689	0.56898
0.0909	0.655	0.65498	0.655	0.65493	0.65498
0.1429	0.732	0.732	0.732	0.73196	0.732
0.2	0.8021	0.80213	0.8021	0.80215	0.80213
0.3333	0.9277	0.92765	0.9277	0.92767	0.92768
0.5	-	1.0389	-	1.0389	1.03907
1	1.2326	-	1.2326	-	1.23258

Table 3. Comparison of the SQLM results of local Nusselt number -θ(0) for normal fluid (φ_v=0) for various values of Pr with Sc=1,m=λ=Sr=Df=Grt=Grc=Ec=Yc=Nr=κ=A=0.

			-θ’(0)		
1.0389	**Chamkha et al. [32]**	**Yih [33].**	**Ullah et al.**	**Nageeb et al.**	**Present**
1	0.33217	0.332057	0.332	0.332057	0.332057
10	0.72831	0.728141	0.7281	0.728141	0.72814
100	1.57218	1.571831	1.5718	1.571658	1.571754
1000	3.38809	3.387083	3.3881	3.396962	3.392166
10000	7.3008	7.297402	7.3102	7.351156	7.298394

Table 4. Values of the skin friction coefficient f “(0), local Nusselt number θ’(0) and local Sherwood number φ’(0) for Cu, Ag and Al_2O_3 water based nanofluid with Pr=6.2, Sc=1, m=λ=Sr=Df=Grt=Grc=Ec=Yc=Nr=κ=0, Bi1=Bi2=0.5 for various values of A and φ_v.

		− f”(0)				**−θ’(0)**			**−φ’(0)**	
A	**φ_v**	**Cu**	**Ag**	**Al_2O_3**	**Cu**	**Ag**	**Al_2O_3**	**Cu**	**Ag**	**Al_2O_3**
0	0.05	0.5207	0.5352	0.4721	0.6339	0.637	0.6148	0.3631	0.366	0.3528
	0.1	0.5517	0.5753	0.469	0.6008	0.6039	0.5716	0.3692	0.3737	0.3521
	0.2	0.572	0.6057	0.4489	0.5197	0.5199	0.4843	0.379	0.3791	0.3475
	0.05	0.8594	0.8832	0.7791	0.7131	0.7158	0.6935	0.3973	0.4	0.3874
0.2	0.1	0.9104	0.9494	0.774	0.6725	0.6748	0.643	0.4031	0.4073	0.3868
	0.2	0.9439	0.9995	0.7408	0.5766	0.5752	0.5419	0.4067	0.4124	0.3823
	0.05	1.4805	1.5215	1.3422	0.8129	0.8151	0.793	0.439	0.4415	0.4299
0.8	0.1	1.5683	1.6355	1.3334	0.7624	0.7636	0.733	0.4442	0.448	0.4293
	0.2	1.6261	1.7219	1.2762	0.6473	0.6436	0.614	0.4475	0.4526	0.4252

Table 5. Values of the skin friction coefficient -f''(0), local Nusselt number -θ'(0) and local Sherwood number−φ'(0) for Ag and Al_2O_3 water based nanofluid with φ_v=0.1 and Pr=6.2, Sc=1, A=0.8, λ=0.1, Bi1=Bi2=0.5, Grt=Grc=0.01 for various physical parameters.

β	κ	Nr	Yc	Wc	Df	Sr	-f''(0)		-θ'(0)		-φ'(0)	
							Ag	Al_2O_3	Ag	Al_2O_3	Ag	Al_2O_3
0.2	0.5	0.5	0.5	0.3	0.2	0.3	1.6638	1.3996	0.0889	0.1916	0.9506	0.9081
0.5	-	-	-	-	-	-	1.7072	1.427	0.3803	0.487	1.0801	1.0327
1	-	-	-	-	-	-	1.7784	1.4726	0.7197	0.8324	1.2653	1.2111
0.5	0.2	-	-	-	-	-	1.6531	1.3619	0.3973	0.5064	1.0724	1.0232
-	0.5	-	-	-	-	-	1.7072	1.427	0.3803	0.487	1.0801	1.0327
-	0.8	-	-	-	-	-	1.7596	1.4893	0.3636	0.4681	1.0875	1.0419
-	0.5	0.1	-	-	-	-	1.7068	1.4267	0.159	0.4047	1.1605	1.0729
-	-	0.5	-	-	-	-	1.7072	1.427	0.3803	0.487	1.0801	1.0327
-	-	1	-	-	-	-	1.7075	1.4273	0.4072	0.4689	1.0598	1.0255
-	-	0.5	0.1	-	-	-	1.7067	1.4267	0.8294	0.8434	0.962	0.9406
-	-	-	0.5	-	-	-	1.7072	1.427	0.3803	0.487	1.0801	1.0327
-	-	-	1	-	-	-	1.7077	1.4274	−0.1817	0.0411	1.2278	1.1479
-	-	-	0.5	0.3	-	-	1.7072	1.427	0.38026	0.487	1.08007	1.0327
-	-	-	-	0.5	-	-	1.707	1.4269	0.3635	0.4698	1.1592	1.1134
-	-	-	-	0.8	-	-	1.7069	1.4268	0.3398	0.4455	1.2698	1.2259
-	-	-	-	0.3	0.2	-	1.7072	1.427	0.3803	0.487	1.08007	1.0327
-	-	-	-	-	0.5	-	1.7075	1.4273	0.1301	0.2541	1.1398	1.0877
-		-	-	-	0.8	-	1.708	1.4276	−0.1778	−0.0318	1.2152	1.1572
-	-	-	-	-	0.2	0.3	1.7072	1.427	0.3803	0.487	1.0801	1.0327
-	-	-	-	-	-	0.5	1.7073	1.4271	0.3691	0.4821	1.1057	1.0341
-	-	-	-	-	-	1	1.7076	1.4274	0.3328	0.4651	1.12	1.0537

It is found that the skin-friction coefficient is slightly increased by increasing the value of β, κ, Nr, Ec, Df and Sr. The local Nusselt number is increased as β and Nr are increased while it is decreased as the value of κ, Ec, Yc, Df and Sr are increased. Further, the local Sherwood number is enhanced as the value of β, κ, Ec, Yc, Df and Sr are increased.

Figures 2-4 shows the effect of nanoparticle volume fraction ν on the velocity, temperature, and concentration profiles for Ag water based nanofluids for both steady and unsteady flow [29].

Increasing ν leads to increase the fluid velocity and temperature profiles while it decreases the concentration profiles for both steady and unsteady flow. Greater temperature and concentration distributions are observed in the steady flow than unsteady flow, whereas the opposite trend is observed for the velocity distribution. Further, it is noticed that greater the value of ν leads to enhance the thermal boundary layer thickness while it leads to decline the momentum and concentration boundary layer thickness. Figures 5-7) display the influence of the unsteadiness parameter A on velocity, temperature, and concentration profiles respectively for both Ag and Al_2O_3 water based nanofluids [30].

It demonstrates that the velocity profiles are an increasing function while the temperature and concentration profiles are decreasing function of A. This leads to reduce the thickness of the momentum, thermal, and concentration boundary layer. It is also observed that the lower temperature and concentration distributions, 9 and the higher velocity distribution in Ag than in Al_2O_3 water based nanofluid as increasing the value of A [31]. The effect of the pressure gradient parameter β on the velocity, temperature, and concentration profiles are shown respectively in Figures 8-10.

It illustrates that the velocity profiles rises while the temperature and concentration profiles decline as β increases. This is due to the growth of wedge angle the fluid moves much slow and diminishes the thickness of velocity, temperature and concentration boundary layer. The effect of permeability parameter κ on the velocity profile is shown in Figure 9. It is also noticed that the increment of κ leads to enhance the velocity of the nanofluid on the porous surface and reduce its boundary layer thickness. Figures 10 and 11 respectively show the effect of thermal radiation parameter Nr and Eckert number Ec on the temperature profiles [32,33].

As Nr increases near the boundary surface, the temperature profiles increase correspondingly up to a certain range, and after that it shows the opposite trend. The temperature profiles also increase near the boundary surface and attain a peak value for large Ec, and then reduce in the rest of the region. This suggests that the thermal boundary layer become thicker with increasing value of Ec. The effect of the Dufour number D f on the temperature profiles is shown in Figure 12.

Greater the value of Df leads to an increment of the temperature profiles. Dufour effect is the heat transfer brought by volume fraction gradients and substantial because of the density variance in the flow system. Figure 13 shows the effect of the chemical reaction parameter Yc on the concentration profiles.

The concentrations profiles reduce with an increment of Yc. Similar trends are observed for both Df and Yc as pointed out in [16]. Figure 14 reveal that increasing the value of Soret number Sr leads to increase the concentration profiles and its boundary layer thickness except near the boundary surface.

This enrichment of concentration profiles is due to the mass flux generated by the temperature gradient. Figure 15 displays that the velocity profiles are increasing function of moving wedge parameter λ.

This implies that when wedge moves the fluid velocity at the surface of the wedge is no longer equal to the initial fluid velocity. Figures 16 and 17 display the effect of Biot numbers Bi1 and Bi2 on temperature and nanoparticle concentration fields respectively.

The increment of Bi1 leads to increase the sheet surface and the nanofluid temperature. The intensity of convective heating on the sheet surface increases when the value of Bi1 increases. This leads to the growth of convective heat transfer from the hot fluid on the lower surface of the sheet to the nanofluid on the upper surface which intern enhance the thickness of thermal boundary layers. From Figure 17 it is realized that the sheet surface and nanofluid concentration increase with an increases in the value of Bi2.

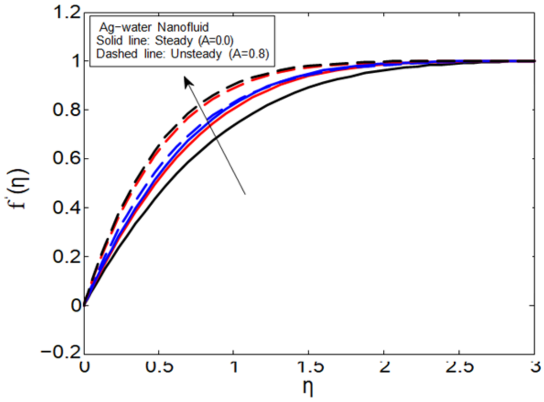

Figure 2. Velocity profiles for various values of φ_v. **Note:** ( ) φ_v=0.0, ( ) φ_v=0.1, ( ) φ_v=0.2, ( ) φ_v=0.0, ( ) φ_v=0.1, ( ) φ_v=0.2.

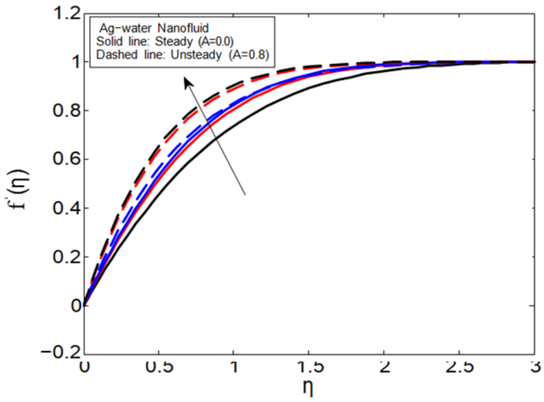

Figure 3. Temperature profiles for various values of φ_v. **Note:** ( ) φ_v=0.0, ( ) φ_v=0.1, ( ) φ_v=0.2, ( ) φ_v=0.0, ( ) φ_v=0.1, ( ) φ_v=0.2.

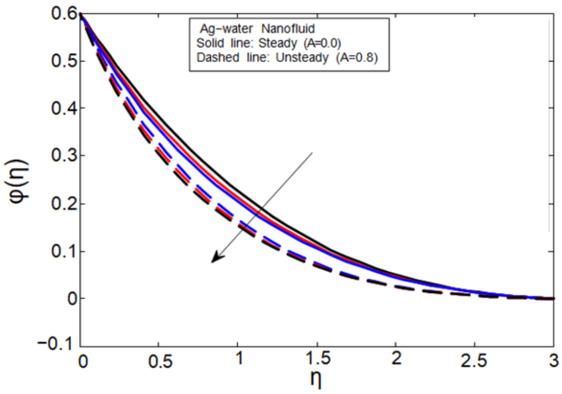

Figure 4. Concentration profiles for various values of φ_v. **Note:** ( ) φ_v=0.0, ( ) φ_v=0.1, ( ) φ_v=0.2, ( ) φ_v=0.0, ( ) φ_v=0.1, ( ) φ_v=0.2.

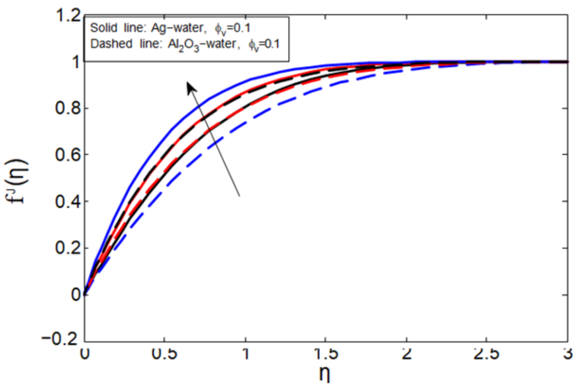

Figure 5. Velocity profiles for various values of A. **Note:** ( ) A=0.0, ( ) A=0.1, ( ) A=0.2, ( ) A=0.0, ( ) A=0.1, ( ) A=0.2.

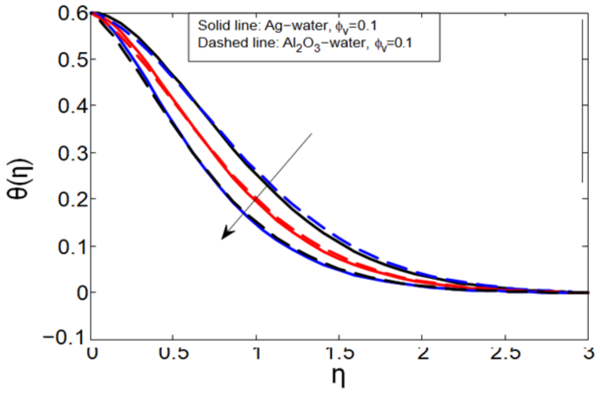

Figure 6. Temperature profiles for various values of A. **Note:** (———) A=0.0, (———) A=0.1, (———) A=0.2, (— —) A=0.0, (— —) A=0.1, (— —) A=0.2.

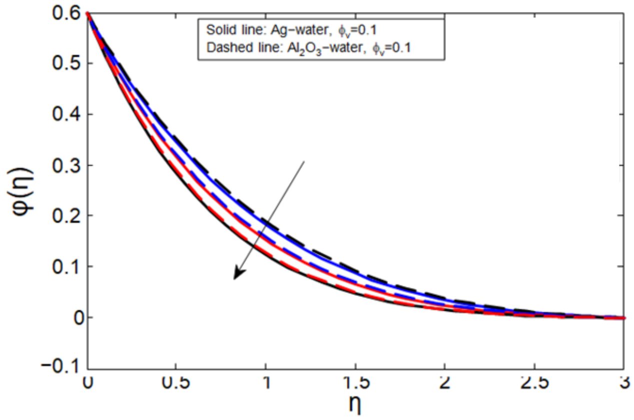

Figure 7. Concent profiles for various values of A. **Note:** (———) A=0.0, (———) A=0.1, (———) A=0.2, (— —) A=0.0, (— —) A=0.1, (— —) A=0.2.

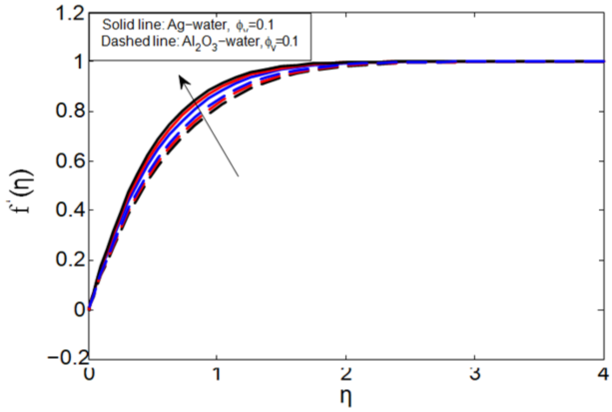

Figure 8. Velocity profiles for various values of β. **Note:** (———) β=0.0, (———) β=0.1, (———) β=0.2, (— —) β=0.0, (— —) β=0.1, (— —) β=0.2.

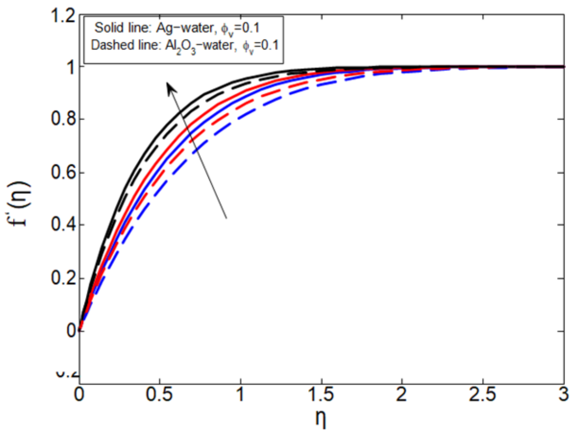

Figure 9. Velocity profiles for various values of κ. **Note:** (———) κ=0.0, (———) κ=0.1, (———) κ=0.2, (— —) κ=0.0, (— —) κ=0.1, (— —) κ=0.2.

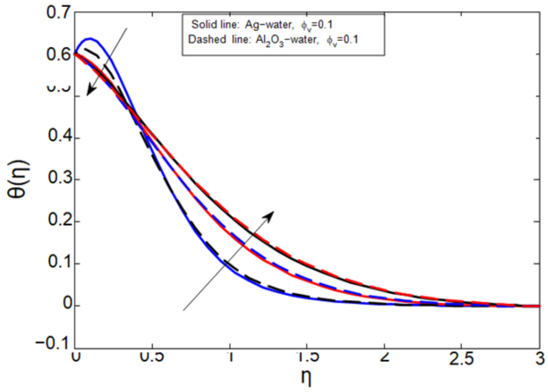

Figure 10. Temperature profiles for various values of Nr. **Note:** (——) Nr=0.0, (——) Nr=0.1, (——) Nr=0.2, (— —) Nr=0.0, (— —) Nr=0.1, (— —) Nr=0.2.

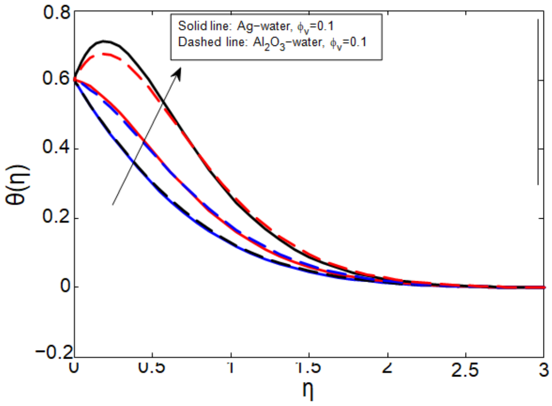

Figure 11. Temperature profiles for various values of Ec. **Note:** (——) Ec=0.0, (——) Ec=0.1, (——) Ec=0.2, (— —) Ec=0.0, (— —) Ec=0.1, (— —) Ec=0.2.

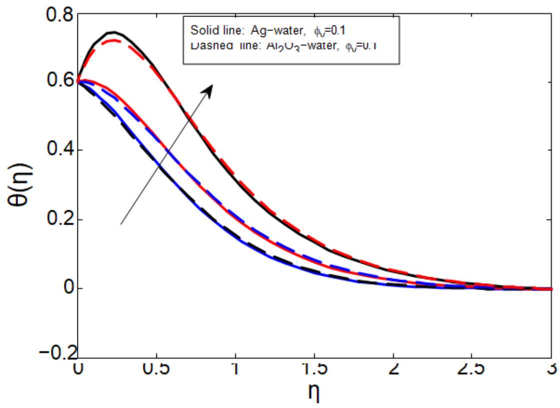

Figure 12. Temperature profiles for various values of Df. **Note:** (——) Df=0.0, (——) Df=0.1, (——) Df=0.2, (— —) Df=0.0, (— —) Df=0.1, (— —) Df=0.2.

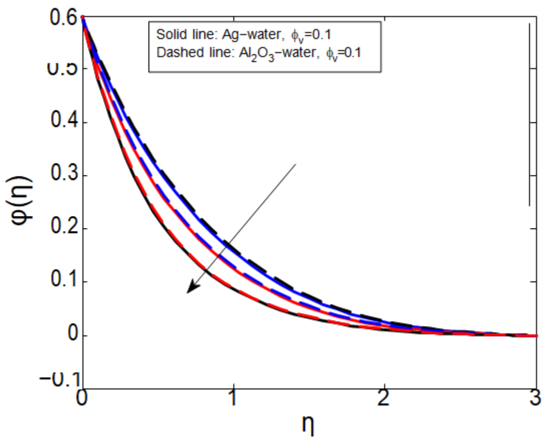

Figure 13. Concent profiles for various values of Yc. **Note:** (——) Yc=0.0, (——) Yc=0.1, (——) Yc=0.2, (— —) Yc=0.0, (— —) Yc=0.1, (— —) Yc=0.2.

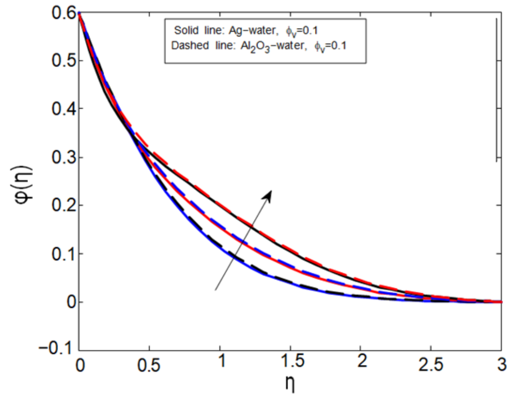

Figure 14. Concent profiles for various values of Sr. **Note:** (———) Sr=0.0, (———) Sr=0.1, (———) Sr=0.2, (— —) Sr=0.0, (— —) Sr=0.1, (— —) Sr=0.2.

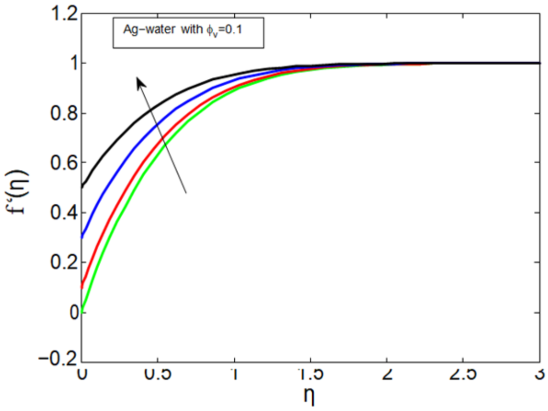

Figure 15. Velocity profiles for various values of λ. **Note:** (———) λ=0.0, (———) λ=0.1, (———) λ=0.2, (— —) λ=0.0, (— —) λ=0.1, (— —) λ=0.2.

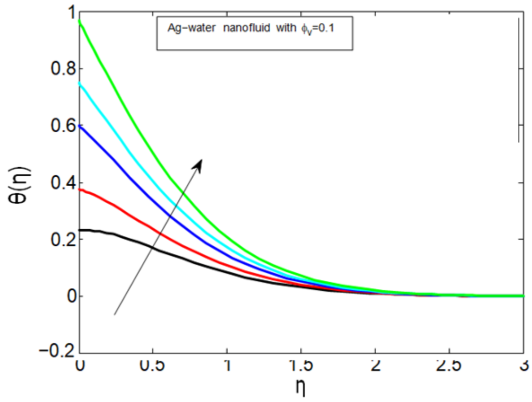

Figure 16. Temperature profiles for various values of Bi_1. **Note:** (———) Bi_1=0.0, (———) Bi_1=0.1, (———) Bi_1=0.2, (— —) Bi_1=0.0, (— —) Bi_1=0.1, (— —) Bi_1=0.2.

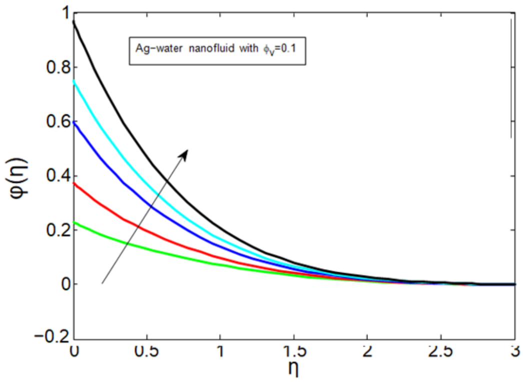

Figure 17. Concen profiles for various values of Bi_2. **Note:** (———) Bi_2=0.0, (———) Bi_2=0.1, (———) Bi_2=0.2, (— —) Bi_2=0.0, (— —) Bi_2=0.1, (— —) Bi_2=0.2.

Conclusion

Unsteady mixed convection heat and mass transfer boundary layer flow of nanofluid past a moving wedge in porous media is studied. The flow of Cu, Ag and Al_2O_3 water based nanofluids are considered and assumed that the nanoparticle volume fraction can be actively controlled at the boundary surface. The governing equations were numerically solved using SQRM. From the obtained results the following conclusions are drawn:

The nanofluid velocity and temperature profiles reduce with increasing the values of nanoparticle volume fraction while the opposite behavior is observed for concentration distribution.

Greater values of temperature and concentration distributions are perceived in the steady flow than unsteady flow whereas the opposite trend is seen for the velocity distribution. The nanofluid velocity, temperature and concentration distributions are respectively increasing functions of moving wedge parameter, thermal and solutal Biot numbers. The skin fraction coefficient and local Sherwood number are increasing functions while the local Nusselt number is a decreasing function of the nanoparticle volume fraction, permeability parameter, Eckert number, and the Soret number. For Al_2O_3 water based nanofluids, the skin friction coefficient, local Nusselt number, and local Sherwood number are decreasing functions of nanoparticle volume fraction.

Acknowledgment

The authors wish to express their thanks to Prof. S.S. Motsa for his valuable contribution in usage of SQRM for the solution of the paper.

Conflicts of Interest

The authors declare that they have no conflicts of interest.

Funding Statement

There is no funding for conducting this research article.

References

1. Choi, US, and Jeffrey A Eastman. "Enhancing thermal conductivity of fluids with nanoparticles." *Argonne National Lab*.(ANL), Argonne, IL (United States) (1995).
2. Ellahi, R. "The effects of MHD and temperature dependent viscosity on the flow of non-Newtonian nanofluid in a pipe: Analytical solutions." *Appl Math Modell* 37 (2013): 1451-1467.
3. Salahuddin T, Arif Hussain, MY Malik, M Awais, and Mair Khan. "Carreau nanofluid impinging over a stretching cylinder with generalized slip effects: Using finite difference scheme." *Result Phys* 7 (2017): 3090-3099.
4. Makinde OD, Fazle Mabood WA Khan, and MS Tshehla. "MHD flow of a variable viscosity nanofluid over a radially stretching convective surface with radiative heat." *J Mol Liq* 219 (2016): 624-630.
5. Ibrahim, Wubshet, and Bullo Hindebu. "Magnetohydrodynamic (MHD) boundary layer flow of eyring-powell nanofluid past stretching cylinder with cattaneo-christov heat flux model." *Nonlinear Eng* 8 (2019): 303-317.
6. Khan, Md Shakhaoath, Ifsana Karim, Md Sirajul Islam, and Mohammad Wahiduzzaman. "MHD boundary layer radiative, heat generating and chemical reacting flow past a wedge moving in a nanofluid." *Nano Converg* 1 (2014): 1-13.
7. Srinivasacharya D, Upendar Mendu and K Venumadhav. "MHD boundary layer flow of a nanofluid past a wedge." *Procedia Eng* 127 (2015): 1064-1070.
8. Xu, Xiaoqin, and Shumei Chen. "Dual solutions of a boundary layer problem for MHD nanofluids through a permeable wedge with variable viscosity." *Bound Value Probl* (2017): 1-13.
9. BK Ramesh, RK Shreenivas, LN Achala, and NM Bujurk. Similarity solutions of the MHD flow past a constant wedge within porous media, Hindawi. Math *Prob Eng* (2017).
10. Alam MS, M Ali, MA Alim, MJ Haque Munshi, and MZ Uddin Chowdhury. "Solution of Falkner-Skan unsteady MHD boundary layer flow and heat transfer past a moving porous wedge in a nanofluid." *Procedia Eng* 194 (2017): 414-420.
11. Pal, Dulal, and Gopinath Mandal. "Mixed convection–radiation on stagnation-point flow of nanofluids over a stretching/shrinking sheet in a porous medium with heat generation and viscous dissipation." *J Pet Sci Eng* 126 (2015): 16-25.
12. Rosali, Haliza, Anuar Ishak, Roslinda Nazar, and Ioan Pop. "Mixed convection boundary layer flow past a vertical cone embedded in a porous medium subjected to a convective boundary condition." *Propuls Power Res* 5 (2016): 118-122.
13. Haile, Eshetu, and Bandari Shankar. "Boundary-layer flow of nanofluids over a moving surface in the presence of thermal radiation, viscous dissipation and chemical reaction." *Appl Appl Math* 10 (2015): 21.
14. Ibrahim, Wubshet, and Ayele Tulu. "Magnetohydrodynamic (MHD) boundary layer flow past a wedge with heat transfer and viscous effects of nanofluid embedded in porous media." *Math Prob Engi* (2019).
15. AC Yunus, and AJ Ghajar. Heat and mass transfer, fundamentals and applications. Fifth Edi Pub by Mcgraw-Hill Edu.
16. Haroun, Nageeb AH, Sabyasachi Mondal, and Precious Sibanda. "Effects of thermal radiation on mixed convection in a MHD nanofluid flow over a stretching sheet using a spectral relaxation method." *Int J Math Comput Sci* 11 (2017): 52-61.
17. Chakraborty, Tanmoy, Kalidas Das, and Prabir Kumar Kundu. "Ag-water nanofluid flow over an inclined porous plate embedded in a non-Darcy porous medium due to solar radiation." *J Mech Sci Technol* 31 (2017): 2443-2449.
18. Majety, Syam Sundar, and K. Gangadhar. "Viscous dissipation effects on radiative MHD boundary layer flow of nano fluid past a wedge through porous medium with chemical reaction." *IOSR J Math* 12 (2016): 71-81.
19. Motsa, Sandile Sydney. "A new spectral local linearization method for nonlinear boundary layer flow problems." *J Appl Math* (2013).
20. Motsa SS, andZG Makukula, S Shateyi. "Spectral local linearisation approach for natural convection boundary layer flow." *Math Prob Eng* (2013).
21. Oyelakin, Ibukun Sarah, Sabyasachi Mondal, and Precious Sibanda. "Unsteady Casson nanofluid flow over a stretching sheet with thermal radiation, convective and slip boundary conditions." *Alex Eng J* 55 (2016): 1025-1035.
22. Ullah, Imran, Ilyas Khan, and Sharidan Shafie. "Heat and mass transfer in unsteady MHD slip flow of Casson fluid over a moving wedge embedded in a porous medium in the presence of chemical reaction: Numerical Solutions using Keller-Box Method." *Numer Methods Partial Differ Equ* 34 (2018): 1867-1891.
23. Versteeg, Henk Kaarle, and Weeratunge Malalasekera. "An introduction to computational fluid dynamics: The finite volume method." *Pearson education* (2007).
24. Ullah I, Khan I, Shafie S. "Hydromagnetic Falkner-Skan flow of Casson fluid past a moving wedge with heat transfer." *Alex Eng J* 55(2016): 2139-2148.
25. Ali, Naser, Joao A. Teixeira, and Abdulmajid Addali. "A review on nanofluids: Fabrication, stability, and thermophysical properties." *J Nanomat* (2018).
26. Hady F, Mohamed R Eid, and Mostafa A Ahmed. "Slip effects on unsteady MHD stagnation point flow of a nanofluid over stretching sheet in a porous medium with thermal radiation." *J Pure Appl Math: Adv Appl* 12 (2014): 181-206.
27. Yirga Y, and B. Shankar. "MHD flow and heat transfer of nanofluids through a porous media due to a stretching sheet with viscous dissipation and chemical reaction effects." *Int J Computat Met Eng Sci Mecha* 16 (2015): 275-284.
28. Trefethen, Lloyd N. "Spectral methods in matlab." *Soc indus appl math* (2000).
29. Ashwini G, and AT Eswara. "MHD Falkner-Skan boundary layer flow with internal heat generation or absorption." *Int J Math Com Sci* 6 (2012): 556-559.

30. Watanabe T. “Thermal boundary layers over a wedge with uniform suction or injection in forced flow.” *Acta Mechanica* 83 (1990): 119-126.
31. Ganapathirao M, R Ravindran, and E. Momoniat. “Effects of chemical reaction, heat and mass transfer on an unsteady mixed convection boundary layer flow over a wedge with heat generation/absorption in the presence of suction or injection.” *Heat Mass Trans* 51 (2015): 289-300.
32. Chamkha Ali J, Mir Mujtaba A Quadri, and Camille Issa. “Thermal radiation effects on MHD forced convection flow adjacent to a non-isothermal wedge in the presence of a heat source or sink.” *Heat Mass Trans* 39 (2003): 305-312.
33. Yih KA “MHD forced convection flow adjacent to a non-isothermal wedge.” *Int Commun Heat Mass Trans* 26 (1999): 819-827.

How to cite this article: Tulu, Ayele and Wubshet Ibrahim "Unsteady Mixed Convection Flow, Heat and Mass Transfer of Nanofluid past a Moving Wedge Embedded in a Porous Medium." *J Appl Computat Math* 11(2022):480